sciendo

ANNALS OF WEST UNIVERSITY OF TIMISOARA PHYSICS
Vol. LXIII, 2021

DOI: 10.2478/awutp-2021-0004

FIRST-PRINCIPLES CALCULATIONS OF THE STRUCTURAL, ELECTRONIC AND OPTICAL PROPERTIES OF YTTRIUM-DOPED SnO_2

Nabil Beloufa[1], Youcef Chechab[1], Souad Louhibi-Fasla[1], Abbes Chahed[2], Samir Bekheira[3], Hamza Rekab-Djabri[1,4], Salah Daoud[5]

[1]*Laboratory of Micro and Nanophysics (LaMiN), National Polytechnic School Oran, ENPO-MA, BP 1523, El M'Naouer, 31000, Oran, Algeria.*
[2]*Condensed Matter and Sustainable Development Laboratory (LMCDD), University of Sidi Bel-Abbes, Sidi Bel-Abbes 22000, Algeria*
[3]*Laboratory of Materials (LabMat), National Polytechnic School Oran, ENPO-MA, BP 1523, El M'Naouer, 31000, Oran, Algeria.*
[4]*Faculty of Nature and Life Sciences and Earth Sciences, Akli Mohand-Oulhadj University, 10000, Bouira, Algeria*
[5]*Laboratory of Materials and Electronic Systems, Mohamed El Bachir El Ibrahimi University of Bordj Bou Arreridj, Bordj Bou Arreridj, 34000, Algeria*
**Corresponding author: Email: faslasouad0@gmail.com*

Article Info

Received: 26.04.2021
Accepted: 14.06.2021

Keywords:
FP-LAPW, Y-doped SnO_2, Reflectivity, Absorption

Abstract

We use FP-LAPW method to study structural, electronic, and optical properties of the pure and Y-doped SnO_2. The results show that by Y doping of SnO_2 the band gaps are broadened, and still direct at Γ-point. For pure SnO_2 material, the obtained values of the direct band gap are 0.607 eV for GGA-PBE and 2.524 eV for GGA-TB-mBJ, respectively. This later is in good agreement with the experimental data and other theoretical results. The Fermi level shifts into the valence band and exhibits p-type semiconductor character owing mainly from the orbital 4d-Y. Additionally, the calculated optical properties reveal that all concentrations are characterized by low reflectivity and absorption via wavelength λ (nm) in the visible light and near-infrared (NIR) ranges, which leads to a redshift in the optical transparency.

1. Introduction

Transparent and conductive oxides (TCO) such as tin dioxide (SnO_2), zinc oxide (ZnO) and indium oxide (In_2O_3) are a class of materials that have a high optical transparency in the visible wavelength range, and high reflectance in the infrared (IR) with good electrical conductivity [1, 2]. Tin dioxide (SnO_2) is a unique material with important properties such as high thermal stability and a high degree of transparency in the visible

region of the spectrum. It is also an important n-type semiconductor with wide band energy (3.6-3.8 eV) [3]. Due to its excellent optical, electrochemical and catalytic properties, it is used in many practical applications such as semiconductor sensors, solar cells [4], lithium batteries and optoelectronic devices [5,6]. The SnO_2 similar to other energetic wide band gap materials such as TiO_2, SiO_2 and ZnO, it exhibits good photo-catalytic and antibacterial activity as well as degradability of organic contaminants [7]. Bolzan*et al.* [8] and Chetri*et al.* [9] conducted experiments to determine the structural parameters of SnO_2. Different experimental techniques [10-12] have been used to observe high-pressure phase transitions in SnO_2.

Very many impurities for doping SnO_2 thin films have been applied by other researchers such as Fluorine (F) [13], Antimony (Sb), Copper (Cu), Nickel (Ni) [14], Cobalt (Co), etc. According to the literature, SnO_2 doped with metallic elements [15,16] could give rise to the ideal electronic device where the crystallinity, electrical conductivity and optical properties of doped SnO_2 films are improved compared to undoped layers. In accordance to the current n-type doping of SnO_2 [17], p- type SnO_2 could be used to create new semiconductor device applications.

Doping with various elements, including Sb [16, 18], Zn [19], Li [20], In [21], and Ga [22] have been used to obtain different results. In fact, M.Boujnah *et al*. [23] reported that the 3d transition metals (Sc, Ti and V) doped rutile SnO_2 exhibits a new transparent conducting oxide with p-type semiconducting valuable for solar cells. Yttrium (Y) doped TiO_2, it's found to be successful in improving photo catalytic activity and extending the absorption edge towards visible light [24-26]. Furthermore, the 4d transition metals (Y, Ag, Cd, Nb, Mo) doped TiO_2 reduce the energy gap of rutile TiO_2, leading to same redshift in the optical absorption edge [27] with photocalytic activity being evidently enhanced [28]. In the previous studies, the Y doped ZnO can enhance the UV emission and decrease the deep level emission (DLE) band in the green range of ZnO [28-31], which doping with Y ions reduces the nonradioactive recombination centers and increase the possibility of the near band edge transition of ZnO. Yttrium ion is suitable to incorporate in SnO_2, giving a similar crystalline size of Y^{3+}cation to Sn^{4+}, and leading good dispersion and enhance separation of electron-hole pairs [24].

The objective of this work is to study the influence of doping (6.25% and 12.5%) of yttrium on the structural, electronic and optical properties of tin dioxide (SnO_2). The presentation of our work consists of three parts. In the first section, we make a general introduction on the properties of transparent conducting oxide (TCO), including tin dioxide.

The second part is concerned with the computational method and details used in this work. The third section shows our results and discussion for structural, electronic and optical properties of Y doped SnO_2. Finally, this work has been completed by a conclusion.

2. Computational method and details

The structure of SnO_2 is similar to the rutile-type, with the space group $P4_2/mnm$; the unit cell is tetragonal quadratic with the experimental lattice parameters a = b = 4.738Å and c = 3.187Å [32,33]. The unit cell contains six atoms: two tin atoms and four oxygen atoms. Sn atoms are in position 2a: (1/2; 1/2; 1/2) and (0; 0; 0) and O atoms are in position 4f, given by (u ; u ; 0), (1-u ; 1-u ; 0), (1/2+u ; 1/2-u ; 1/2-u ; 1/2) and (1/2-u ; 1/2+u ; 1/2), respectively, with u = 0.3056 [8]. The calculations have been performed by the method of linearized augmented plane waves (FP-LAPW), within the framework of the Density Functional Theory (DFT) using the code Wien2K [34]. For the treatment of exchange potential and correlation, the approximation of the generalized gradient (GGA) as developed by Perdew, Burke and Ernzerhof [35] was used. However, for the electronic and optical properties, theTrans-Blaha modified Becke-Johnson potential (TB-mBJ) [36] was also applied. For the region of muffin-tin spheres we used to ensure the Convergence of spherical harmonics l_{max}=10, the wave functions in the interstitial region are extended into plane waves with a cut-off energy $R_{MT}\times k_{max}$= 9 (where R_{MT} is the small radius of the muffin-tin spheres. The criterion of convergence of self-consistent cycles is only reached when the total energy is stable at 0.1 mRy [37]. The structures were geometrically optimized until the residual atomic energy is less than 0.01 eV/Å and the total energy is less than 10^{-5}eV/atom, respectively.

The cut-off energy that defines the separation between core and valence states is taken-10 Ry. The core states are treated within the framework of complete relativism, while the valence states are treated within the framework of scalar relativism. Since we have a semiconductor and non-magnetic material, spin-orbit coupling effects are neglected because of their very small effect on the calculation of the different properties. Muffin-Tin radii (R_{MT}) was taken equal to 2.12, 1.90, 1.70 u.a for Sn, Y, and O atoms, respectively. The electronic configuration of Tin is [Kr] $4d^{10}$ $5s^2$ $5p^2$, Yttrium is [Kr] $4d^1$ $5s^2$ and that of Oxygen [He] $2s^2$ $2p^4$.

3. Results and discussions

3.1. Structural properties

We were performed all calculations with Y doped 2×2×2 super-cell, which contains 48 (32-Sn atoms and 16-O atoms). The percentage of doping used is 6.25 and 12.5%, the doping at 0.0625 is obtained by replacing one atom of Y in the site of Sn, and the doping at 0.125 is achieved at the same super-cell by injecting two atoms of Y into the site of Sn by substitution (show Figure1). The arguments for choosing this dopant are presented in the first section, we note that the atomic radius of the Yttrium impurity R (Y^{3+}) = 1.005 Å is very close to that of the tin atom Sn R (Sn^{4+}) = 1.11 Å, so it is almost constant. The structure keeps the same symmetry. We take the most stable phase, which is the rutile phase. The results are obtained using the FP-LAPW method implemented in the WIEN2K code.

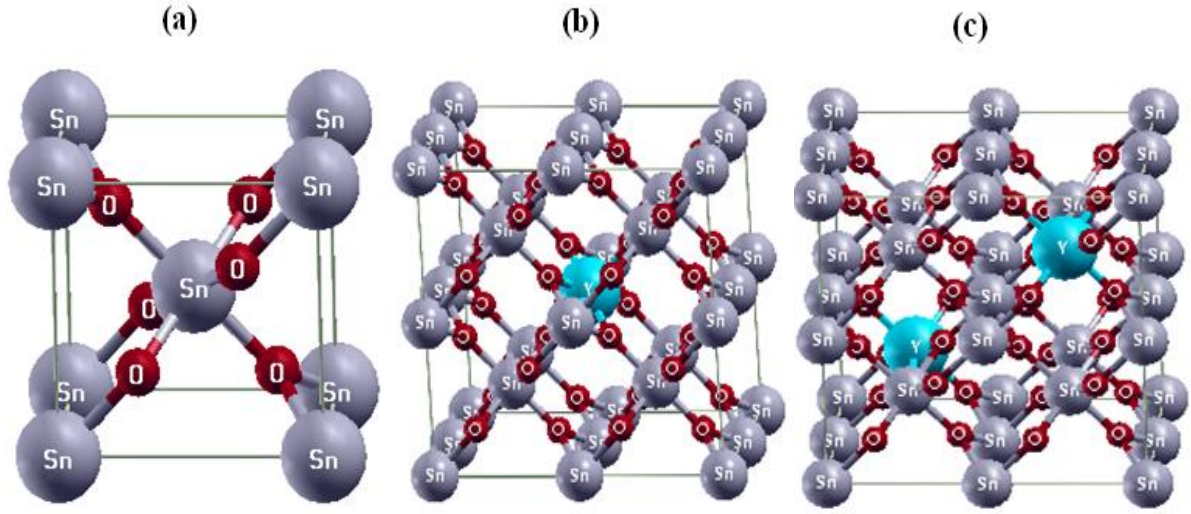


Figure 1. Structure of : (a) pure SnO_2 , (b) $Y_{0.0625}Sn_{0.9375}O_2$, and (c) $Y_{0.125}Sn_{0.875}O_2$

Tin oxide is crystallized in the tetragonal structure. So, the calculation consists of making an optimization of *c*/*a* ratio, internal parameter *u* and volume *V*, this optimization is used to determine the optimal values of lattice parameters, the compressibility module and its pressure derivative.

We have calculated the variation of the total energy as a function of unit cell volume, and the obtained curve was fitted to the Murnaghan's equation of state [38, 39].

$$E(V) = E_0 + \left[\frac{B_0 V}{B'(B'-1)}\right].\left[B'\left(1-\frac{V_0}{V}\right)+\left(\frac{V_0}{V}\right)^{B'}-1\right] \quad (1)$$

where, *E* and *V* are the total energy and the volume of the unit cell, respectively, E_0 and V_0 are the energy and the volume of the unit cell at equilibrium, respectively, and B_0 and B_0' are

the modulus of compressibility at equilibrium and its first derivative with respect to pressure, respectively.

The modulus of compressibility B_0 and its pressure derivative B_0' are expressed as follow [39]:

$$B_0 = V\frac{\partial^2 E}{\partial V^2} \quad (2)$$

$$\acute{B_0} = \frac{\partial B}{\partial P} \quad (3)$$

The lattice constant a_0(Å) was calculated by the following relation:

$$a_0 = \left(\sqrt[3]{\frac{V_0}{c/a}}\right) \quad (4)$$

These equations allowed us to obtain the equilibrium lattice parameters, the compressibility modulus and the corresponding pressure derivative at the equilibrium. The calculated results are shown in Table 1. The obtained values of the lattice parameters for pure SnO_2 are a_0 = 4.831Å, c = 3.233 Å, c/a = 0.671, and u = 0.306, respectively. They are in good agreement with the other theoretical results [40-50] and the values obtained from the experience [51, 52]. Our value of the B_0 = 197.39GPa is slightly higher than B_0 = 181 GPa calculated by Peltzer y Blanc *et al.* [40], and lower than the value B_0 = 244.7 GPa found by Zhu *et al.* [41]. The doped materials have the rutile-type structure of tetragonal symmetry. Small changes were observed in the volume and in the lattice parameters of the crystalline structures. Figure 2 illustrates the optimization curve for pure SnO_2 (a), $Y_{0.0625}Sn_{0.9375}O_2$ (b), and $Y_{0.125}Sn_{0.875}O_2$ (c), respectively.

With the increase of the Y concentration in $Y_xSn_{1-x}O_2$ (x=0, 0.0625, 0.125), the lattice constants a, c and the calculated volume are also increased. The variation of the lattice parameters is due to a minor difference of the ion radii between them. The ion radius of Y^{3+} (0.89Å) is greater than that of Sn^{4+} (0.69 Å), therefore, the lattice constant increased after the doping process.

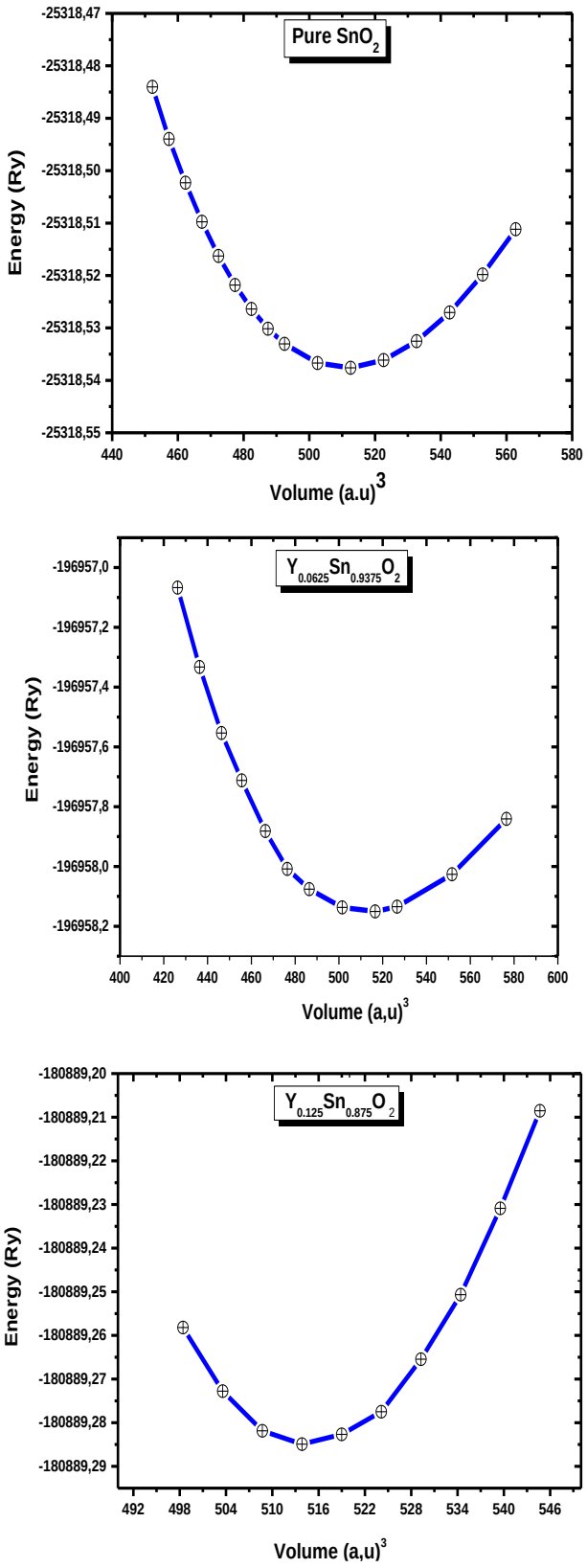


Figure 2. The variation of total energy as a function of volume for $Y_xSn_{1-x}O_2$ with x = 0, 6.25% and 12.5% using GGA.

Table 1. Equilibrium structural parameters: a_0 (Å), c (Å), c/a, internal parameter u, unit cell volume V (Å^3), bulk modulus B_0 (GPa) and its pressure derivative B_0' at zero pressure of $Y_xSn_{1-x}O_2$ (x=0, 0.0625, 0.125), in comparison with other calculations and the available data of experiments.

System	a_0 (Å)	c (Å)	c/a	u	V (Å)^3	B_0(GPa)	E_{coh}(eV)
SnO_2	4.831*	3.233*	0.671*	0.306*	75.83*	197.39*	26.073*
		3.288[a]	0.673 [a]	0.307[e]	78.44[h]	204.5[a]	
		3.194[b]	0.672[d]	0.306[f]0.3061[g]	68.76[i]	244.7[f]	
		3.236[c]			71.49[j]	181[k]	
		3.186[m]				212[l]	
$Y_{0.0625}Sn_{0.9375}O_2$	4.847*	3.252*	0.672*	0.344*	76.57*	187.19*	26.888*
$Y_{0.125}Sn_{0.875}O_2$	4.871*	3.301*	0.677*	0.346*	78.34*	145.28*	27.287*

*Present calculations,

[a]Ref. [42], [b]Ref. [43], [c]Ref. [44], [d]Ref. [45], [e]Ref. [46], [f]Ref. [41], [g]Ref. [40] , [h]Ref. [47], [i]Ref. [48], [j]Ref. [49], [k]Ref. [50], [l]Ref. [51]Experiment, [m]Ref. [52]Experiment.

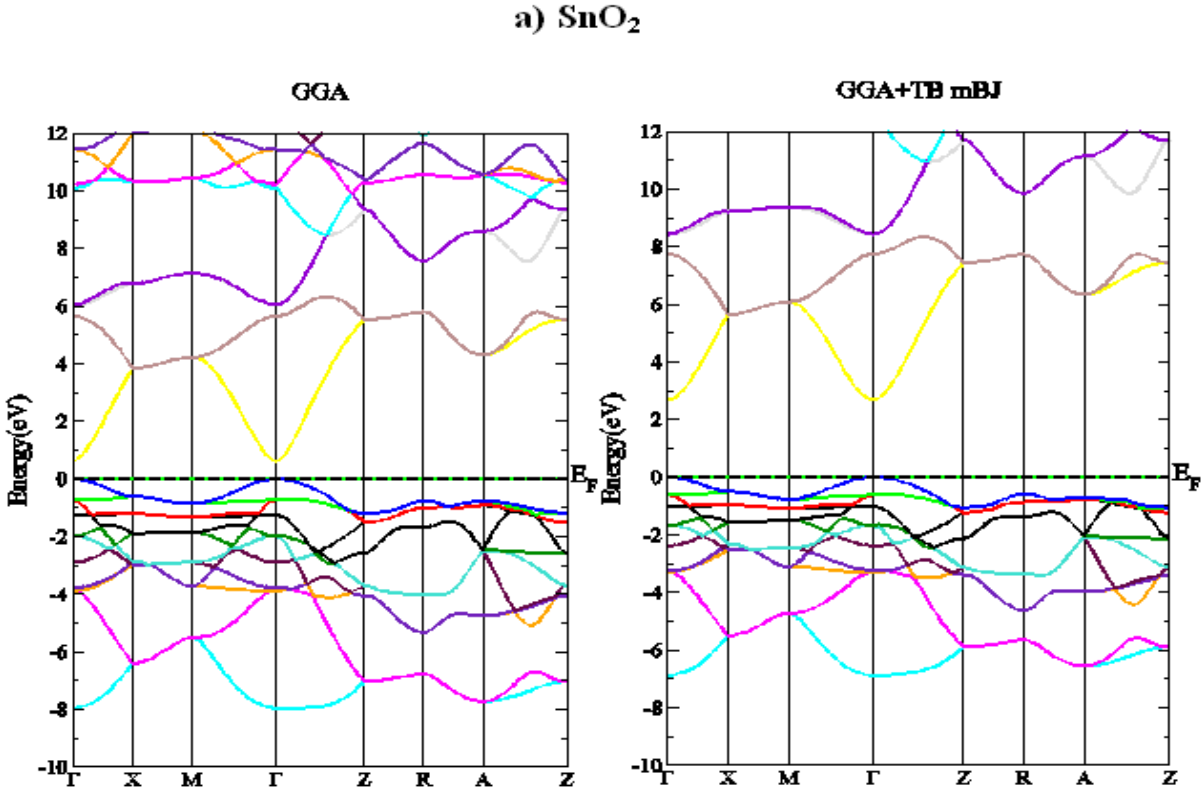
3.2. Electronic properties.

3.2.1. Band structure

The combination of the En (k) curves represent the electron dispersion curves in the crystal: also known as the band structure. In the same way that it is necessary to know V(r) on the elementary cell of the crystal; the curves En (k) have the same symmetry as the reciprocal space and it is sufficient to describe En(k) in the first Brillouin zone. We have calculated the band structure of $Y_xSn_{1-x}O_2$ with (x=0, 0.0625 and 0.125) with the GGA and GGA + TB-mBJ approximations, using the FP-LAPW method. We have plotted this band structure following the points and directions of high symmetry in the first Brillouin zone. The corresponding band structure is shown in Figure 3.

Both the maximum and minimum of the valence and conduction bands are expressed as follow the point of high symmetry Γ, indicating a direct transition (Γ-Γ). The table 2 contains the different gap values of the studied compounds calculated by the approximation GGA and GGA + TB-mBJ and compared with other results. The difference between the value of the gap obtained from GGA-PBE and that of the experiment is due to usual underestimation of GGA for the energy gaps compared to those of the experiment. To overcome this problem, we have used the method named TB-mBJ, which has the role of correcting the gap to confront the experimental values. We note that our results of pure SnO_2 are very comparable to experimental data. To the best of our knowledge, neither experimental nor theoretical data

related to electronic properties of $Y_{0.0625}Sn_{0.9375}O_2$ and $Y_{0.125}Sn_{0.875}O_2$ materials are available. When an Y^{3+} substitutes the Sn^{4+} in the SnO_2 host lattice, it leaves one hole in the valence band and contributes to offset the relative position of the Fermi level with respect to the top of the valence band. This leads to acceptor-like energy band around the VBM. Hence Y doped SnO_2 is an extrinsic semiconductor with a p-type conduction characteristic in the ideal diluted system. However, experimentally the charge neutrally is disturbed due to this replacement, hence the system search the neutral configuration with the compensation of vacancies, which is not taken in the present work.



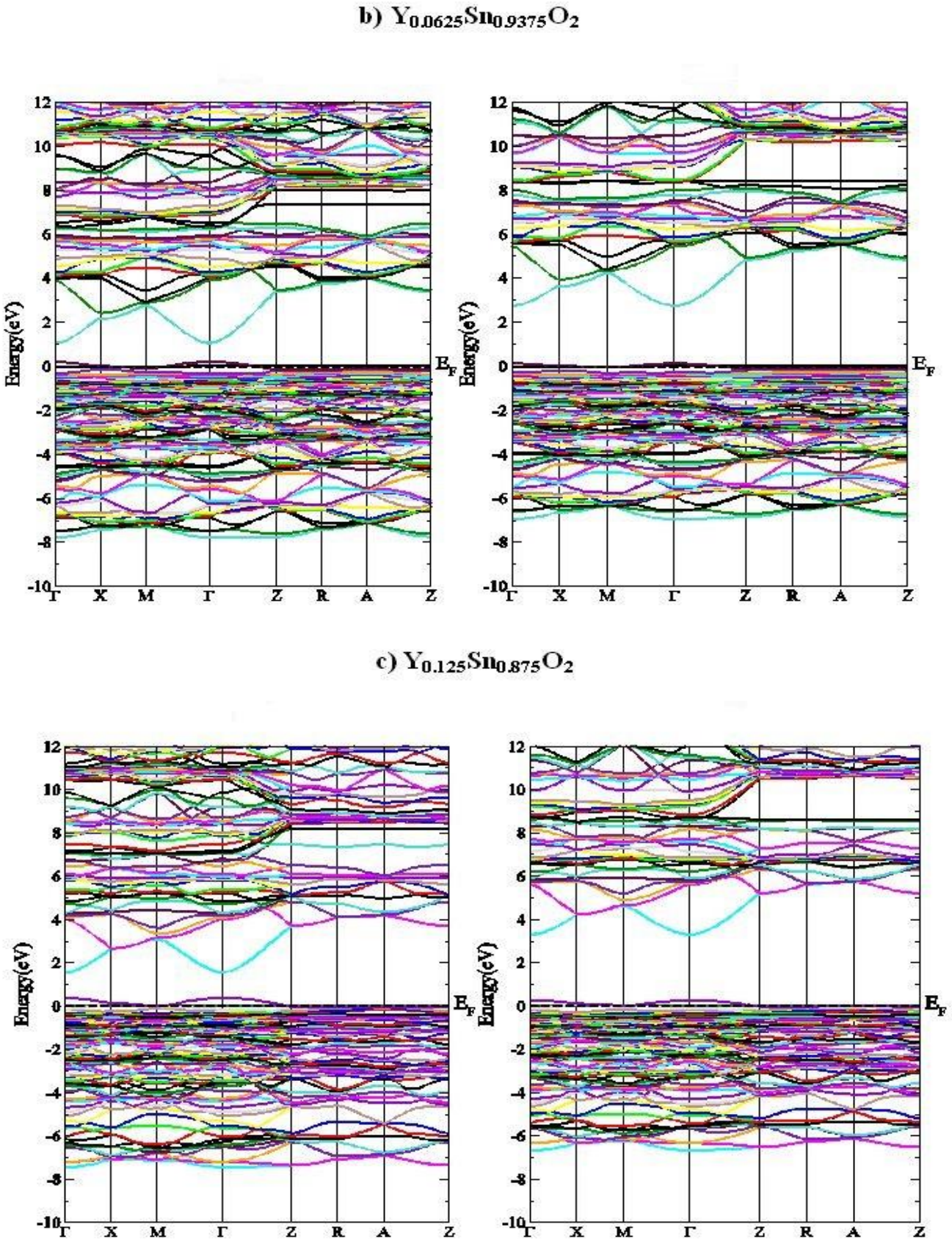


Figure 3. Band structures of pure SnO_2 (a),$Y_{0.0625}Sn_{0.9375}O_2$ (b), and $Y_{0.125}Sn_{0.875}O_2$ (c) using GGA(left panel) and GGA+ TB-mBJ (right panel).

Table2: Calculated band gap of $Y_xSn_{1-x}O_2$(x=0, 0.0625 and 0.125) with GGA and GGA + TB-mBJ approximations, compared with the theoretical and experimental values.

Gap energyEg (eV)					
Compound	This work		Other works		Experimental results
	GGA	TB-mBJ	GGA	TB-mBJ	
SnO_2	0.607	2.524	1.07 [45] 0.832[55]	2.84[45] 2.86[54] 2.76[55]	2.76 [45]3.6 [53]
$Y_{0.0625}Sn_{0.9375}O_2$	0.843	2.678	-	-	-
$Y_{0.125}Sn_{0.875}O_2$	0.933	2.847	-	-	-

3.2.2 Density of state (DOS)

The density of states of these compounds is calculated by the tetrahedron method [56], which requires a large number of special points in the Brillouin zone. A number of 168 special points is used for pure SnO_2 semiconducting material, while 87 points is used for the other concentrations. The total and partial densities of states (TDOS and PDOS) of pure and yttrium doped SnO_2 with concentrations 6.25% and 12.5% are presented in Figure 4. For pure SnO_2 the valence band is dominated by a mixing between the Sn-5s and Sn-4d states and the O-2p state. The conduction band is derived mainly from the Sn-5s and O-2p. In the case of doped SnO_2, a Fermi level shift appears in the valence band. In the vicinity of the Fermi level it is characterized mainly by Y-4d and may be responsible firstly for the extrinsic electrical conductivity caused by the doping of SnO_2 by yttrium. Concerning the valence band, we see that the region between -8 eV and 0 eV is characterized by Sn-5s, Y-4d and O-2p with a small contribution of Sn-4d states. The conduction band is derived mainly from Sn-5s and Y-4d.

From Figure 5, the existence of O-2p states over the Fermi level suggests a shift of charge balance between the metallic and oxide lattice sites, such that the lower valency of Y^{+3} compared to Sn^{+4} contributes to shifts of the Fermi level into the valence band. The impurity levels are introduced above the Fermi energy and it situated at about 0.18 eV (0.21 eV) for 6.25% (12.5%) doping concentrations. We observed that the magnitude of impurity levels increases with the Y concentrations and is consistent with the difference of valence between Sn and Y, and indicates that each Y dopant offers a hole as a charge carrier in the SnO_2 host lattice. In addition, the position of conduction band edge move slightly to higher energy in the band gap structure. This situation is observed in the SnO_2 doped Scandium [23] which the band gap becomes bigger than the band gap of pure SnO_2. The main reason in the broadening of the band gap are the 2p-O and Sn-5s orbitals that operate in the top of VBM and the bottom of CBM respectively affecting by Yttrium doping.

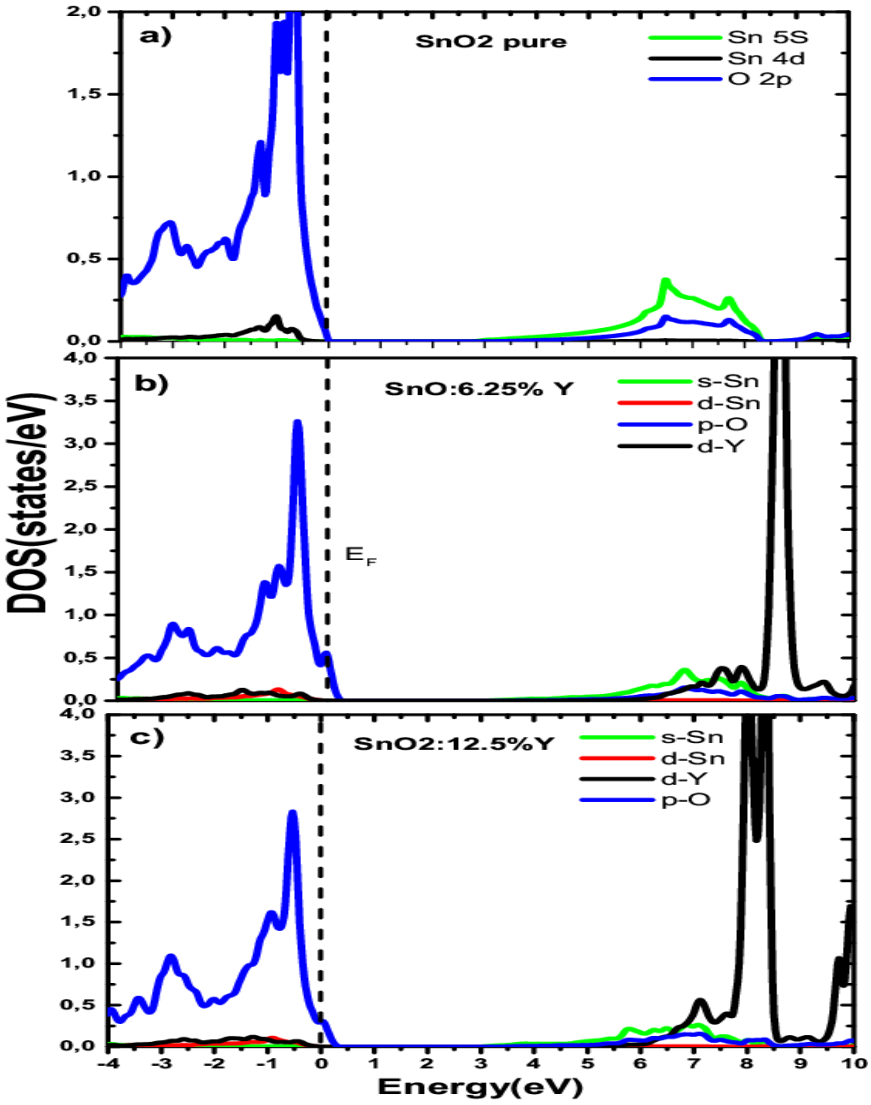


Figure 4. Total and partial DOS of(a) pure SnO_2,(b)$Y_{0.0625}Sn_{0.9375}O_2$, and (c) $Y_{0.125}Sn_{0.875}O_2$using GGA+ TB-mBJ

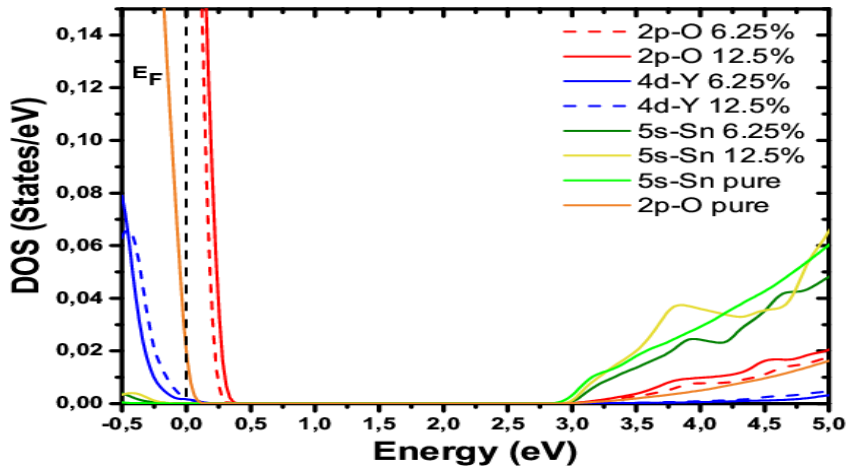


Figure 5. Compared orbitals in the top VBM and bottom CBM using GGA+ TB-mBJ

3.4. Optical properties

The optical properties of a material subjected to the effect of an external excitation (radiation) are described by the dielectric function ε(ω). The determination of the real and imaginary parts of the dielectric function allows us to evaluate other important optical properties, such as optical absorption refractive index and reflectivity. The measurable quantity that represents an important observable in the optical properties is the dielectric function ε (ω) of the system where it is presented in complex form by [57]

$$\varepsilon(\omega) = \varepsilon_1(\omega) + i\varepsilon_2(\omega) \tag{5}$$

with the real part $\varepsilon_1(\omega)$ describing polarization, which represents the dispersion of the incident photons by the materials and the imaginary part $\varepsilon_2(\omega)$ describing absorption, which results from the inter-band transition between the occupied states in the valence band and the unoccupied states in the conduction band, the both quantities are related by the Kramers-Kronig equations [59,60]:

$$\varepsilon_1(E) = 1 + \frac{2}{\pi}\int_0^\infty \frac{E'\varepsilon_2(E')}{E'^2 - E^2} dE' \tag{6}$$

$$\varepsilon_2(E) = -\frac{2E}{\pi}\int_0^\infty \frac{\varepsilon_1(E')}{E'^2 - E^2} dE' \tag{7}$$

where $E = \hbar\omega = h\nu.$ design the photon energy. The Kramers–Krönig relations permit us to determine either the real or the imaginary component if the other is known for all frequencies. $\varepsilon_2(\omega)$ is evaluated from momentum matrix elements given by the following relation [61]:

$$\varepsilon_2(\omega) = \frac{4\pi^2 e^2}{3m^2\omega^2}\sum_{v,c}\int_{BZ}\frac{2dk}{(2\pi)^3}\left|\langle ck|P_I|vk\rangle\right|^2 \delta\left(E_c(k) - E_v(k) - \hbar\omega\right) \tag{8}$$

where *c*, *v* and P_I represents conduction band, valence band and momentum operator respectively. $|vk\rangle, \langle ck|$ represents the Bloch functions for the valence band and conduction band respectively. The summation is done on all the states of the irreducible zone of Brillouin (IBZ).The optical constants can be extracted from the knowledge of $\varepsilon_1(\omega)$ and $\varepsilon_2(\omega)$ using the following relation

$$n(\omega) = \frac{1}{\sqrt{2}}[(\varepsilon_1(\omega)^2 + \varepsilon_2(\omega)^2)^{1/2} + \varepsilon_1(\omega)\ ]^{1/2} \quad (9)$$

$$R(\omega) = \left|\frac{\sqrt{\varepsilon(\omega)} - 1}{\sqrt{\varepsilon(\omega)} + 1}\right|^2 = \frac{(n-1)^2 + k^2}{(n+1)^2 + k^2} \quad (10)$$

$$\alpha(\omega) = \frac{4\pi}{\lambda} k(\omega) \quad (11)$$

wherein (ω), R(ω), α(ω) and K(ω) denoted the refraction index, Reflectivity, Absorption coefficient and Extinction index respectively.

Figure 6 illustrate the variation of the real and imaginary part of the dielectric function as a function of the different yttrium doping concentrations. The energy threshold for pure SnO_2 is 1.109 eV, which corresponds to the transition between O-2p located at the valence band maximum and Sn-5s located at the conduction band maximum and the threshold energy equals for the doping case to 0.106 eV and 0.094 eV for the concentration 6.25% and 12.5%, respectively. This decrease in energy is effectively due to the increase of occupied states. The first peak energy for the 6.25% Y concentration observed in the imaginary part (ε_2) is a value of 0.237 eV, it is dominated by the electronic transition from the acceptor states the Y-4d state to the unoccupied states of the conduction band above the Fermi level. This means that the electrical conductivity of Yttrium-doped SnO_2 can improve from low excitation energy, which is useful for transparent conducting electrode device. However, the first peak energy is dislocated in 0.289eV for the 12.5% yttrium concentration.

The reflectivity of light is important in the calculation of optical properties; it is sensitive to the complicated combination of the dielectric function. We present a performance comparison between the reflectivity curves of pure SnO_2 and doped with 6.25 and 12.5% as a function of wavelength (Figure 7(a)). All concentrations show low average reflectivity less than 15% in the visible light and UV regions and less in the near infrared region. The Figure 7(a) shows oscillations in reflectivity, which decrease with the Y concentrations. Figure 7(b) shows the variation of absorption coefficient as a function of wavelength λ(nm) for 0%, 6.25% and 12.5% Yttrium concentrations. It is confirmed that all concentrations are characterized by low absorption in the visible and near infrared region. It can be seen that the 6.25% concentration shows slightly low absorption compared to the 12.5% concentration. Low reflectivity together with low absorption in the visible light and near infrared regions leads to considered transmittance of undoped SnO2, regarding the

experimental data on the SnO_2 rutile thin film [62,63] shows an excellent optical transparency along the visible range with an average of 83%. Regarding to the experiments when we considered all conditions, the decreasing transmittance results at increasing Yttrium doping. In fact, the increasing Y^{3+}doping levels induces to the increasing of scattering of photon through its crystal defects mainly the oxygen vacancies created by doping, hence the absorption edge gradually shifted to a low energy region [64]. Changmin et *al*. [65] reported that the dopant Y could successfully control the free carrier concentration by suppressing the formation of oxygen vacancy inside SnO_2 semiconductors due to its lower electronegativity (1.22) and standard electrode potential (-2.38V) with increasing Y to fabricate Y-doped SnO_2 thin film transistor [65]. While, in the ideal diluted system, the results allow us to assess that the transmittance of doped SnO_2 can be gradually increases in the visible light and near infrared (NIR) ranges owing to the low absorption and the area reflectivity in this range. Furthermore, the optical transmittance enhances with incorporation of Y dopant that is required for transparent conducting application.

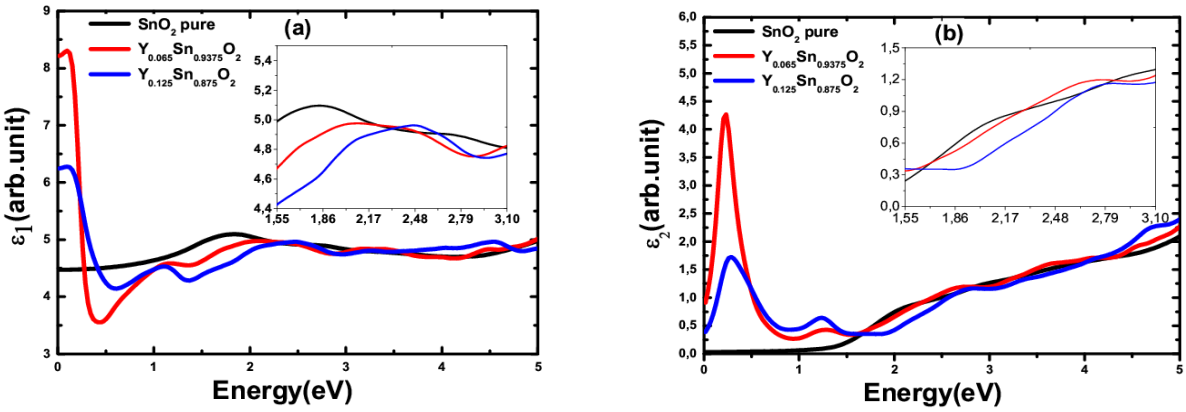


Figure 6. Real part(a) and imaginary part(b) of the dielectric function of pure SnO_2 and SnO_2Y-doped with 6.25 and 12.5%, using GGA+TB-mBJ

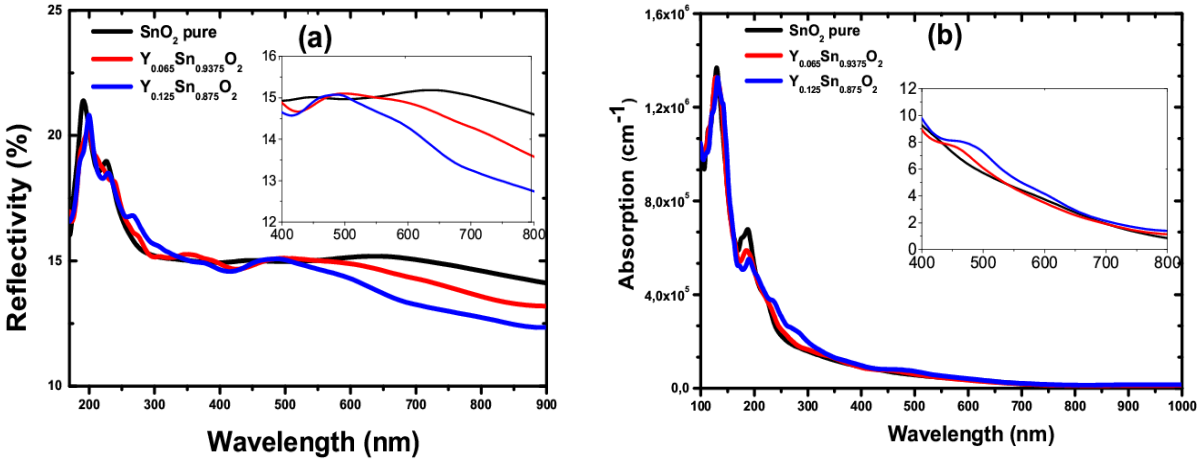


Figure 7. Reflectivity(a) and absorption (b) as a function of the wavelength (λ) of pure SnO_2, SnO_2Y-doped with 6.25 and 12.5%, using GGA+TB-mBJ.

4. Conclusion

We have investigated the structural, electronic and optical of pure and Y-doped SnO_2. We first study the effect of dopant on the host lattice and reveal that the doping of Y element in the SnO_2 lattice induces the increase of the lattice constant. We show, using GGA and mBJ methods that the pure SnO_2 exhibits a direct band gap at Γ point and is in agreement with experimental results. For the doped system, the Fermi level is displaced into the valence band producing a p-type semiconductor characteristic owing to 4d-Y orbital. Additionally, the band gaps are broadened by doping. The optical response shows a low absorption and area reflectivity in visible light and infrared ranges depicting that the intrinsic band gap of SnO_2 was affected by the doping. Furthermore, the optical transmittance enhances with the incorporation of Y dopant that is required for transparent conducting application.

References

[1] Q.-B. Ma, Z.-Z. Ye, H.-P. He, L.-P. Zhu, J.-Y. Huang, Y.-Z. Zhang, B.-H. Zhao, *Scripta Mater.* **58** (2008) 21

[2] W. Daranfed, N. Guermat, I. Bouchama, K. Mirouh, S. Dilmi, M. A. Saeed, *J. Nano- Electron. Phys.* **11** (06) (2019) 6001

[3] B. Straumal, B. Baretzky, A. Mazilkin, S. Protasova, A. Myatiev, P. Straumal, *J. Eur. Ceram. Soc.* **29** (2009) 1963

[4] S. Ramanathan (Ed.), *Thin Film Metal-Oxides: Fundamentals and Applications in Electronics and Energy*, Springer, New York, (2010)

[5] K.H. Tam, A.B. Djurišić, C.M.N. Chan, Y.Y. Xi, C.W. Tse, Y.H. Leung, D.W.T. Au, *Thin Solid Films* **516** (2008) 6167

[6] S.A. Khan, S. Shahid, F. Ijaz, *Green Synthesis of Copper oxide Nanoparticles & Biomedical Application*, Publisher: Lambert Academic Publishing, 1: 1-133 (2017)

[7] P.V. Viet, C.M. Thi, L. V. Hieu, *J. Nanomater.* **2016** (2016) ID 4231046

[8] A.A. Bolzan, C. Fong, B.J. Kennedy, *Acta Crystallogr.* ***B*** **53** (1997) 373

[9] P. Chetri, B. Saikia, A. Choudhury, *Journal of Applied Physics* **113** (2013) 233514

[10] H. Hellwig, A.F. Goncharov, E. Gregoryanz, H. Mao, R.J. Hemley, *Phys. Rev. B***67** (2003) 174110

[11] S. Ono, E. Ito, T. Katsura, A. Yoneda, M.J. Walter, S. Urakawa, W. Utsumi, K.Funakoshi, *Phys. Chem. Miner.***27** (2000) 618

[12] J.Z. Jiang, L. Gerward, J.S. Olsen, *Scripta Mater.* **44** (2001) 1983

[13] S.F. Ahmed, S. Khan, P.K. Ghosh, M.K. Mitra, K.K. Chattopadhyay, *J. Sol–Gel Sci.Technol.* **39** (2006) 241

[14] J. Zhao, X.J. Zhao, J.M. Ni, H.Z. Tao, *Acta Mater.* **58** (2010) 6243

[15] M. Mehdi, B. Mohagheghi, M.S. Saremi, *J. Phys. D: Appl. Phys.* **37** (2004) 1248

[16] J. Ni, X. Zhao, X. Zheng, J. Zhao, B. Liu, *Acta Mater.* **57** (2009) 278

[17] W. Zhou, L.J. Liu, M.Y. Yuan, Q.G. Song, P. Wu, *Comput. Mater. Sci.* **54** (2012) 109

[18] S.H. Yu, W.F. Zhang, L.X. Li, D. Xu, H.L. Dong, *Appl. Surf. Sci.* **286** (2013) 417

[19] J.M. Ni, X.J. Zhao, J. Zhao, *Surf. Coat. Technol.* **206** (2012) 4356

[20] M. Mehdi, B. Mohagheghi, M.S. Saremi, *Semicond. Sci. Technol.* **19** (2004) 764

[21] Z.G. Ji, Z.J. He, Y.L. Song, K. Liu, Z.Z. Ye, *J. Cryst. Growth* **259** (2003) 282

[22] Y.X. Huang, Z.G. Ji, C. Chen, *Appl. Surf. Sci.* **253** (2007) 4819

[23] M. Boujnah, H. Ennaceri, K. Belasfar, A. El Kenz, A. Benyoussef, M. Loulidi, E. Ahmed, *New transparent conducting oxide based on doped SnO_2 for solar cells*, International Renewable and Sustainable Energy conference (IRSEC) (2016) (pp. 229-233), IEEE

[24] J. Liu, R. Yang, S. Li, *J. Rare Earths* **25** (2007) 173

[25] H. Zhang, K. Tan, H. Zheng, Y. Gu, W.F. Zhang, *Mater. Chem. Phys.* **125** (2011) 156

[26] X. Niu, S. Li, H. Chu, J. Zhou, *J. Rare Earths*, **29** (2011) 225

[27] K. Song, X. Han, G. Shao, *J. Alloys Compd.* **551** (2013) 118

[28] P.-T. Hsieh, R.W.-K. Chuang, C.-Q. Chang, C.-M. Wang, S.-J. Chang, *J. Sol–Gel Sci. Technol.* **58** (2011) 42

[29] J. Yang, R. Wang, L. Yang, J. Lang, M. Wei, M. Gao, X. Liu, J. Cao, X. Li, N. Yang, *J. Alloys Compd.* **509** (2011) 3606

[30] M. Gao, J. Yang, L. Yang, Y. Zhang, J. Lang, H. Liu, H. Fan, Y. Sun, Z. Zhang, H. Song, *Superlattices Microstruct*. **52** (2012) 84

[31] T. Jia, W. Wang, F. Long, Z. Fu, H. Wang, Q. Zhang, *Mater. Sci. Eng. B* **162** (2009) 179

[32] L. Singh, M. N. Luwang, S. Srivastava, *New J. Chem.* **38** (2014) 115

[33] X.F. Liu, J. Iqbal, Z.B. Wu, B. He, R.H. Yu, *J. Phys. Chem. C* **114** (2010) 4790

[34] P. Blaha, K. Schwarz, G. K. H. Madsen, D. Kvasnicka and J. Luitz, WIEN2k, *An Augmented Plane Wave Plus Local Orbitals Program for Calculating Crystal Properties*, Vienna University of Technology, Vienna, Austria (2001)

[35] J.P. Perdew, S. Burke, M. Ernzerhof, *Phys. Rev. Lett.* **77** (1996) 3865

[36] F. Tran, P. Blaha, *Phys. Rev. Lett.* **102** (2009) 226401

[37] P. Zhang, X. Tian, G. Cheng, Y. Xie, H. Zhang, Z. Wei, *J. Alloys Compd.* **576** (2013) 31

[38] F.D. Murnaghan, *Proc. Natl. Acad. Sci. USA* **30** (1944) 5390

[39] H. Rekab-Djabri, Manal M. AbdusSalam,S. Daoud,M. Drief, Y. Guermit, S. Louhibi-Fasla, *J. Magnes. Alloy.* **8** (2020) 1166

[40] E.L. Peltzer y Blanc, A. Svane, N.E. Christensen, *Phys. Rev. B* **48** (1993) 15712

[41] B. Zhu, C-M. Liu, M-B. Lv, X-R. Chen, J. Zhu, G-F. Ji, *Physica B* **406** (2011) 3508

[42] C-M. Liu, X-R. Chen, G-F. Ji, *Comput. Mater. Sci.* **50** (2011) 1571

[43] Y. Li, W. Fan, H. Sun, X. Cheng, P. Li, X. Zhao, J. Hao, M. Jiang, *J. Phys. Chem. B* **114** (2010) 1052

[44] I. Erdem, H.H. Kart, T. Cagin, *J. Alloys Compd.* **587** (2014) 638

[45] M. Kashif, T. Munir, A. Hussain, A. Shahzad, A. Rasheed, N. Amin, M. Noreen, W. Hussain, *Dig. J.Nanomater. Bios*. **13** (2018) 875

[46] Z. Zhu, R.C. Deka, A. Chutia, R. Sahnoun, H. Tsuboi, M. Koyama, N. Hatakeyama, A. Endou, H. Takaba, C.A. Del Caprio, M. Kubo, A. Miyamoto, *Phys. Chem. Solids* **70** (2009) 1248

[47] M.A. Ali, A.K.M.A. Islam, *Physica B* **407** (2012) 1020

[48] L. Gracia, A. Beltran, J. Andrés, *J. Phys. Chem. B* **111** (2007) 6479

[49] Q-J. Liu, Z.-T. Liu, Li-P. Feng, *Comput. Mater. Sci.* **47** (2010) 1016

[50] R. Wyckoff, *Crystal Structures*, 2nd ed., *Wiley Interscience*, New York, (1964)

[51] E. Chang, E.K. Graham, *J. Geophys. Res.***80**(1975) 2595

[52] J. Haines, J.M. Leger, *Phys. Rev. B* **55** (1997) 11144

[53] K. Reimann, M. Steube, *Solid State Commun.* **105** (1998) 649

[54] M.A. Bezzerrouk, M. Hassan, R. Baghdad, S. Reguieg, M. Bousmahaa, B. Kharroubi, B. Bouhafs, *Superlattices Microstruct*. **84** (2015) 80

[55] F. El Haj Hassan, S. Moussawi, W. Noun, C. Salameh, A.V. Postnikov, *Comput. Mater. Sci.* **72** (2013) 86

[56] P. E. Blöchl, O. Jepsen, O. K. Andersen, *Phys. Rev. B* **49** (1994) 16223

[57] A. Baida, M. Ghezali, B. Mahfoud, A. Arroussi, S. Louhibi-Fasla, *Phase Transit.* **93** (2020) 865

[58] R. Fouret, P. Derollez, A. Laamyem, B. Hennion, J. Gonzalez, *J Phys. Condens. Matter*. **9** (1997) 6579

[59] R.d. Kronig, *JOSA* **12** (6) 1926) 547

[60] H. Kramers, *Nature* **11**7 (2952) (1926) 774

[61] R. Fouret, P. Derollez, A. Laamyen, B. Hennion, and J. Gonale, *J. Phys. Conden. Matter*. **9** (1997) 6579

[62] Q. Gao, M. Li, Q. Liu, Y. Wang, X. Li, X. Wei, C. Song, J. Wang, J. Liu, G. Shen, G. Han, *Mater. Lett*. **122** (2014) 143

[63] R. Singh, M. Kumar, S. Shankar, R. Singh, A.K. Ghosh, O.P. Thakur, B. Das, *Mater. Sci. Semicond. Process*. **31** (2015) 310

[64] S. Maheswari , M. Karunakaran , K. Kasirajan , L. Bruno Chandrasekar P. Boomi, *Sensors and Actuators A* **31**5 (2020) 112303

[65] L. Changmin, L. Won-Yong, L. Hyunjae, H. Seunghyun, B. Jin-Hyuk, K. In-Man, K. Hongki, K. Kwangeun, J. Jaewon, *Electronics* **9** (2) (2020) 254